molecules

MDPI

Article

Chalcogen Bond Involving Zinc(II)/Cadmium(II) Carbonate and Its Enhancement by Spodium Bond

Na Liu, Xiaoying Xie * and Qingzhong Li *

The Laboratory of Theoretical and Computational Chemistry, School of Chemistry and Chemical Engineering, Yantai University, Yantai 264005, China; liuna_jiayou00@sina.com

* Correspondence: 202007000015@ytu.edu.cn (X.X.); lqz@ytu.edu.cn (Q.L.)

Abstract: Carbonate MCO_3 (M = Zn, Cd) can act as both Lewis acid and base to engage in a spodium bond with nitrogen-containing bases (HCN, $NHCH_2$, and NH_3) and a chalcogen bond with SeHX (X = F, Cl, OH, OCH_3, NH_2, and $NHCH_3$), respectively. There is also a weak hydrogen bond in the chalcogen-bonded dyads. Both chalcogen and hydrogen bonds become stronger in the order of F > Cl > OH > OCH_3 > NH_2 > $NHCH_3$. The chalcogen-bonded dyads are stabilized by a combination of electrostatic and charge transfer interactions. The interaction energy of chalcogen-bonded dyad is less than −10 kcal/mol at most cases. Furthermore, the chalcogen bond can be strengthened through coexistence with a spodium bond in N-base-MCO_3-SeHX. The enhancement of chalcogen bond is primarily attributed to the charge transfer interaction. Additionally, the spodium bond is also enhanced by the chalcogen bond although the corresponding enhancing effect is small.

Keywords: chalcogen bonds; spodium bonds; synergistic effect; QTAIM; NBO

Citation: Liu, N.; Xie, X.; Li, Q. Chalcogen Bond Involving Zinc(II)/Cadmium(II) Carbonate and Its Enhancement by Spodium Bond. *Molecules* **2021**, *26*, 6443. https://doi.org/10.3390/molecules26216443

Academic Editor: Imre Bakó

Received: 24 September 2021
Accepted: 19 October 2021
Published: 26 October 2021

1. Introduction

Zinc and cadmium are two of the most widely used non-ferrous metals because of their unique physical and chemical properties [1]. They have been explored mainly in natural minerals in the form of carbonates. Zincite $ZnCO_3$ and calcite $CdCO_3$ are the most common carbonate rock-forming minerals. MCO_3 (M = Zn, Cd) possesses a planar triangular configuration with *p*-conjugated molecular orbitals, which is similar to $(BO_3)^{3-}$, $(B_3O_6)^{3-}$, and (B_3O_7) [2–4]. MCO_3 has been accepted as a promising material for optical devices in the ultraviolet region due to its fascinating crystal structure, high birefringence, nonlinear optical properties, and transparency [5–7]. Owing to their special electronic energy band structures, these carbonates also have drawn extensive attention in the fields of chemical sensing, luminescence, lithium ion battery anode materials, catalysis, and magnetic materials [8–10]. The spodium bond (SpB) is a non-covalent interaction that occurs between the Group 12 metal atom and a Lewis base [11]. A region with positive molecular electrostatic potentials (MEPs) is found on the metal atomic surface of tetracoordinated molecules $CdBr_2L_2$ and $HgCl_2L_2$ (L = thiourea) [12], thus it can form a SpB with some bases such as CO, CH_3CN, H_2CS, and H_2CO, with interaction energy less than 9 kcal/mol. A SpB was found for bicoordinated molecules [13], which is stronger than the tetracoordinated molecule. Recently, Liu and Li [14] studied the spodium-bonded complexes of MCO_3 (M = Zn, Cd, and Hg) with three N-bases (HCN, $NHCH_2$, and NH_3) and found that they are more bonded than other types of M(II) molecules since the interaction energy exceeds 30 kcal/mol.

Se compound is not only taken as an electron donor in non-covalent interactions owing to its lone pair electrons but also acts as a Lewis acid in chalcogen bond, which is usually used to describe the non-covalent interaction between the σ-hole/π-hole of the seventh main group atom and Lewis bases [15]. The σ-hole bonding interaction was first utilized to describe halogen bonding [16]. Then such σ-hole bonding was extended to molecules containing group VI atoms [17]. This concept was further reviewed and revisited [18,19].

Organoselenium compounds can engage in a chalcogen bond with different electron donors such as N, O, and halogen through an intermolecular or an intramolecular mode [20]. In most cases, the Se···O chalcogen bond is not very strong with interaction energy less than 10 kcal/mol [21]. For the O electron donors, they are often from H_2O and its derivative as well as carbonyl compounds. However, the chalcogen bond between Se compounds and carbonate MCO_3 (M = Zn, Cd) has not been reported.

An important property of a non-covalent interaction is cooperativity, which can be divided into positive and negative cooperativity. When multiple non-covalent interactions coexist in the same system, their strengths will be enhanced or weakened, thus resulting in a cooperative effect. The cooperativity is of great importance in chemical reactions, molecular recognition, and biochemical regulation [22,23]. Some studies showed that the chalcogen bond displays cooperativity with itself [24–26], halogen bond [27], hydrogen bond [28], alkaline-earth bond [29], and cation-π [30] interactions. However, few studies have been performed for the cooperativity of chalcogen bond with spodium bond.

In this study, we explore the chalcogen bond formed by carbonate MCO_3 (M = Zn, Cd) with SeHX (X = F, Cl, OH, OCH_3, NH_2, and $NHCH_3$) to unveil the substituent effect on the strength of chalcogen bond and its origin. Then adding a spodium bond to the M atom of MCO_3 in MCO_3-SeHX, we study the cooperative effect between the chalcogen and spodium bonds, particularly the enhancing effect of spodium bond on the chalcogen bond, and its mechanism is explored by means of MEP and charge transfer. These dyads and triads have been analyzed in the geometries, energetic, AIM, charge transfer, and orbital interaction.

2. Theoretical Methods

All calculations were carried out using the Gaussian 09 program (Gaussian, Inc., Wallingford, CT, USA) [31]. The structures of all monomers and complexes were optimized at the MP2/aug-cc-pVTZ level. Basis set aug-cc-pVTZ-PP including pseudopotential was applied for Zn and Cd atoms to account for relativistic effects [32]. Then, harmonic frequency analysis was performed at the same level to ensure that all structures are minima on the potential energy surfaces. The interaction energy was defined as the energy difference between the complex and the monomers, in which their geometries were taken from the complex. The interaction energies were corrected for the basis set superposition error (BSSE) by the counterpoise procedure of Boys and Bernardi [33].

The wave function analysis-surface analysis suite (WFA-SAS) program [34] was used to analyze the molecular electrostatic potential (MEP) of monomers and dyads on the 0.001e $Bohr^{-3}$ isosurface. Topological properties were derived from the theory of atoms in molecules (AIM) using QTAIM software [35]. Natural bond orbital (NBO) analysis was performed at the HF/aug-cc-pVTZ(PP) level by the NBO5.0 program [36], which can provide some information for charge transfer, while orbital interaction was analyzed using the NBO6.0 program [37]. Multiwfn and VMD [38,39] were utilized to map non-covalent interactions (NCI) [40]. To gain further insight into the nature of the investigated intermolecular interactions, energy decomposition analysis (EDA) was conducted using the GAMESS program [41,42].

3. Results and Discussion

3.1. Chalcogen-Bonded Dyads Involving MCO_3

Figure 1 shows a diagram of 12 chalcogen-boned dyads of MCO_3-SeHX (X = F, Cl, OH, OCH_3, NH_2, and $NHCH_3$, M = Zn^{2+} and Cd^{2+}), respectively represented from ChB-1 to ChB-12. In each dyad, there are both a ChB and a HB, where the ChB is stronger than the HB. Both the ChB and HB jointly maintain the stability of MCO_3-SeHX. Table 1 summarizes their geometric parameters including the angles of X-Se···O (α_1) and Se-H···O (α_2), distances of Se···O (R_{ChB}) and H···O (R_{HB}), and changes of C=O (r_1) and Se-X (r_2) bond lengths. Both α_1 and α_2 angles reflect the direction of ChB and HB, respectively. Both angles vary in ranges of 160–170° and 120–140°, respectively, and the former is bigger than

the latter. Accordingly, the ChB is more easily formed and the HB is weak. Moreover, both angles display a slight dependence on the M atom of MCO_3. Interestingly, both angles vary inversely (Figure S1, Supplementary Materials). That is, the enhancement of ChB is at the sacrifice of the HB weakening, displaying negative cooperativity. Although the ChB is stronger than the HB, R_{ChB} is longer than R_{HB} due to the bigger atomic radius of Se. Both R_{ChB} and R_{HB} become shorter in the $CdCO_3$ complex than in the $ZnCO_3$ analogue since the O atom of $CdCO_3$ has the greater negative MEP [14]. When MCO_3 is fixed, R_{ChB} is shorter in sequence of $NHCH_3$ > NH_2 > OCH_3 > OH > Cl > F, while R_{HB} is longer irregularly. Both C=O and Se-X bonds are lengthened in the complexes, and the Se-X bond suffers the larger elongation than the C=O bond due to the fact that the C=O bond is double and there is an increase of charge density on the Se-X anti-bonding orbital.

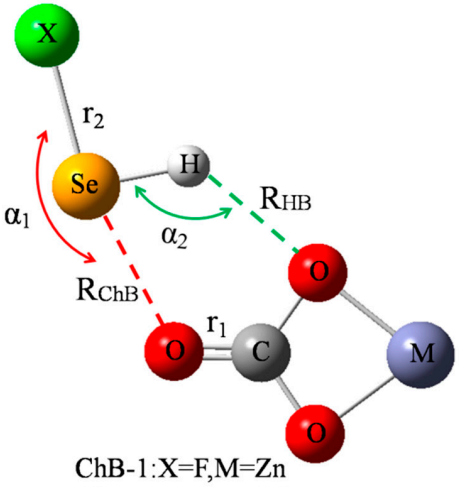

ChB-1:X=F,M=Zn
ChB-2:X=F,M=Cd
ChB-3:X=Cl,M=Zn
ChB-4:X=Cl,M=Cd
ChB-5:X=OH,M=Zn
ChB-6:X=OH,M=Cd
ChB-7:X=OCH_3,M=Zn
ChB-8:X=OCH_3,M=Cd
ChB-9:X=NH_2,M=Zn
ChB-10:X=NH_2,M=Cd
ChB-11:X=$NHCH_3$,M=Zn
ChB-12:X=$NHCH_3$,M=Cd

Figure 1. Scheme of chalcogen-bonded dyad.

The last column of Table 1 lists the interaction energy of chalcogen-bonded dyad, which ranges from −3.6 kcal/mol in ChB-11 to −12.3 kcal/mol in ChB-2. There are some regular variations for the interaction energy. Firstly, for a fixed MCO_3, the interaction energy becomes more negative in the sequence of $NHCH_3$ < NH_2 < OCH_3 < OH < Cl < F, which is consistent with the positive MEPs on the Se and H atoms (Figure 2). Secondly, comparing $SeHOCH_3$ complex with SeHOH analogue, or $SeHNHCH_3$ complex with $SeHNH_2$ analogue, it is found that the methyl group in the chalcogen donor reduces the interaction energy, showing the electron-donating role of the methyl group (confirmed by the increase of positive MEPs on the Se and H atoms). This weakening effect of methyl group is the same as that in the CH···O HB [43]. Thirdly, the interaction energy is larger in the $CdCO_3$ complex than that in the $ZnCO_3$ analogue, evidenced by the more negative MEP on the O atom of $CdCO_3$ [14]. The interaction energy between MCO_3 and SeHX is larger than that with H_2O [44], thus the O atom of MCO_3 is a good electron donor in the chalcogen bond.

Table 1. Angles (α, deg), binding distances (R, Å), change of bond length (Δr, Å), and interaction energy (ΔE, kcal/mol) in the chalcogen-bonded dyads.

	α_1	α_2	R_{ChB}	R_{HB}	Δr_1	Δr_2	ΔE
$ZnCO_3$-SeHF(ChB-1)	169.1	125.0	2.503	2.413	0.011	0.032	−10.35
$CdCO_3$-SeHF(ChB-2)	169.3	124.5	2.451	2.363	0.012	0.040	−12.32
$ZnCO_3$-SeHCl(ChB-3)	166.7	128.8	2.633	2.344	0.009	0.036	−8.52
$CdCO_3$-SeHCl(ChB-4)	167.1	128.2	2.568	2.289	0.010	0.045	−10.29
$ZnCO_3$-SeHOH(ChB-5)	166.7	129.8	2.733	2.438	0.006	0.021	−6.13
$CdCO_3$-SeHOH(ChB-6)	166.9	129.8	2.682	2.380	0.006	0.026	−7.23
$ZnCO_3$-SeHOCH$_3$(ChB-7)	166.8	130.4	2.744	2.437	0.005	0.018	−5.74
$CdCO_3$-SeHOCH$_3$(ChB-8)	166.7	130.5	2.694	2.368	0.006	0.023	−6.82
$ZnCO_3$-SeHNH$_2$(ChB-9)	159.8	138.9	2.969	2.370	0.003	0.015	−3.82
$CdCO_3$-SeHNH$_2$(ChB-10)	160.0	138.9	2.922	2.313	0.003	0.018	−4.48
$ZnCO_3$-SeHNHCH$_3$(ChB-11)	159.8	139.6	2.992	2.361	0.002	0.012	−3.62
$CdCO_3$-SeHNHCH$_3$(ChB-12)	159.2	140.8	2.956	2.286	0.002	0.015	−4.26

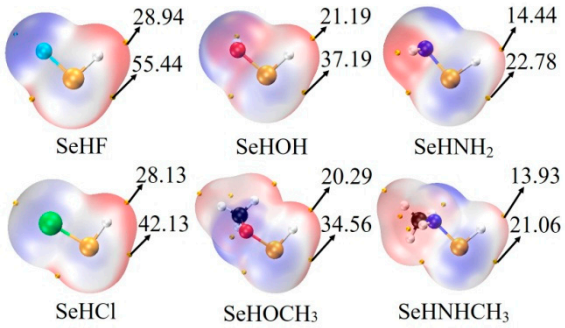

Figure 2. MEP maps on the 0.001 electrons Bohr^{-3} isodensity surface of monomers. Red and blue regions represent positive and negative MEPs, respectively. All are in kcal/mol.

Table 2 lists some important AIM parameters including electron density (ρ), its Laplacian ($\nabla^2\rho$), and energy density (H) at the Se···O BCP in the chalcogen-bonded dyads. ρ is in the range of 0.012–0.035 a.u., and it displays a quadratic relationship with the Se···O distance (Figure 3), with a correlation coefficient of 0.996. Thus the electron density at the Se···O BCP can be used to estimate the change of ChB strength. The trend of density Laplacian is the same as the ρ. H is greater than zero in most dyads except ChB-1, ChB-2, and ChB-4. The negative H in ChB-1, ChB-2, and ChB-4 means that the ChB is a partially covalent interaction, consistent with the larger interaction energy (>10 kcal/mol). Although the AIM parameters of H···O BCP are not analyzed, its coexistence with the ChB is obviously observed in the NCI diagram (Figure S2), where a blue or green area is present between the bonded two atoms.

Table 2. Electron density (ρ), its Laplacian ($\nabla^2\rho$), and energy density (H) at the Se···O BCP in the chalcogen-bonded dyads, all in au.

	ρ	$\nabla^2\rho$	H
ChB-1	0.0312	0.1066	−0.0004
ChB-2	0.0354	0.1143	−0.0017
ChB-3	0.0248	0.0867	0.0010
ChB-4	0.0287	0.0959	0.0002
ChB-5	0.0196	0.0734	0.0016
ChB-6	0.0220	0.0803	0.0013
ChB-7	0.0192	0.0718	0.0016

Table 2. *Cont.*

	ρ	$\nabla^2\rho$	H
ChB-8	0.0216	0.0784	0.0014
ChB-9	0.0126	0.0486	0.0017
ChB-10	0.0140	0.0532	0.0017
ChB-11	0.0121	0.0466	0.0017
ChB-12	0.0133	0.0504	0.0017

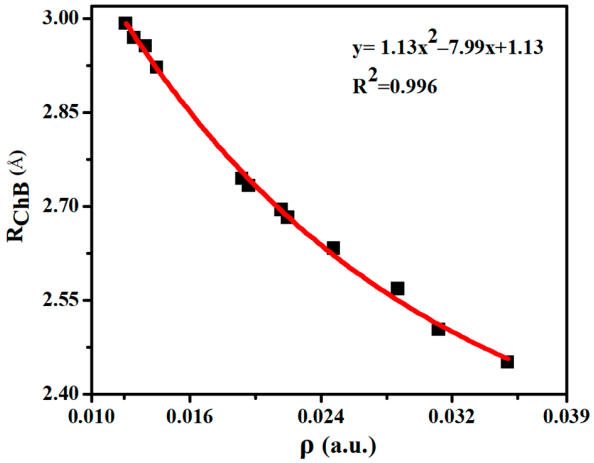

Figure 3. Binding distances (R_{ChB}) versus electron density (ρ) at the Se···O BCP in the chalcogen-bonded dyads.

A charge density moves from MCO_3 to SeHX, which is in a range of 0.009–0.005 e (Table 3). There are two types of ChB and HB in each complex, but the direction of charge transfer is the same for both bonds, thus a linear relationship is present between the interaction energy and charge transfer (Figure 4), with a correlation coefficient of 0.994. For the ChB, the charge transfer is moved from the O lone pair orbital (Lp_O) into the Se-X anti-bonding orbital ($\sigma^*_{Se\text{-}X}$), i.e., $Lp_O \rightarrow \sigma^*_{Se\text{-}X}$. This orbital interaction results in the elongation of the Se-X and C=O bonds. Likely, the perturbation energy of $Lp_O \rightarrow \sigma^*_{Se\text{-}X}$ orbital interaction also displays a linear relationship with the interaction energy (Figure S3). The HB is characterized with an orbital interaction of $Lp_O \rightarrow \sigma^*_{Se\text{-}H}$, which is much weaker than that in the ChB, thus MCO_3-SeHX is primarily stabilized by the ChB. $CdCO_3$ engages in a stronger HB than $ZnCO_3$, confirmed by the larger perturbation energy of $Lp_O \rightarrow \sigma^*_{Se\text{-}H}$ in the $CdCO_3$ complex.

Table 3. Charge transfer (CT, e) and second-order perturbation energies ($E^{(2)}$, kcal/mol) in the chalcogen-bonded dyads.

	CT	Type (ChB)	$E^{(2)}$	Type (HB)	$E^{(2)}$
ChB-1	0.0390	$LP_O \rightarrow \sigma^*_{Se\text{-}F}$	15.12	$LP_O \rightarrow \sigma^*_{Se\text{-}H}$	0.92
ChB-2	0.0493	$LP_O \rightarrow \sigma^*_{Se\text{-}F}$	17.25	$LP_O \rightarrow \sigma^*_{Se\text{-}H}$	1.46
ChB-3	0.0322	$LP_O \rightarrow \sigma^*_{Se\text{-}Cl}$	10.21	$LP_O \rightarrow \sigma^*_{Se\text{-}H}$	0.63
ChB-4	0.0404	$LP_O \rightarrow \sigma^*_{Se\text{-}Cl}$	12.41	$LP_O \rightarrow \sigma^*_{Se\text{-}H}$	1.08
ChB-5	0.0180	$LP_O \rightarrow \sigma^*_{Se\text{-}O}$	5.85	$LP_O \rightarrow \sigma^*_{Se\text{-}H}$	0.25
ChB-6	0.0232	$LP_O \rightarrow \sigma^*_{Se\text{-}O}$	6.32	$LP_O \rightarrow \sigma^*_{Se\text{-}H}$	0.42
ChB-7	0.0186	$LP_O \rightarrow \sigma^*_{Se\text{-}O}$	5.92	$LP_O \rightarrow \sigma^*_{Se\text{-}H}$	0.26
ChB-8	0.0237	$LP_O \rightarrow \sigma^*_{Se\text{-}O}$	6.11	$LP_O \rightarrow \sigma^*_{Se\text{-}H}$	0.40
ChB-9	0.0091	$LP_O \rightarrow \sigma^*_{Se\text{-}N}$	2.58	$LP_O \rightarrow \sigma^*_{Se\text{-}H}$	0.13
ChB-10	0.0120	$LP_O \rightarrow \sigma^*_{Se\text{-}N}$	2.63	$LP_O \rightarrow \sigma^*_{Se\text{-}H}$	0.14
ChB-11	0.0092	$LP_O \rightarrow \sigma^*_{Se\text{-}N}$	2.42	$LP_O \rightarrow \sigma^*_{Se\text{-}H}$	0.14
ChB-12	0.0118	$LP_O \rightarrow \sigma^*_{Se\text{-}N}$	2.50	$LP_O \rightarrow \sigma^*_{Se\text{-}H}$	0.14

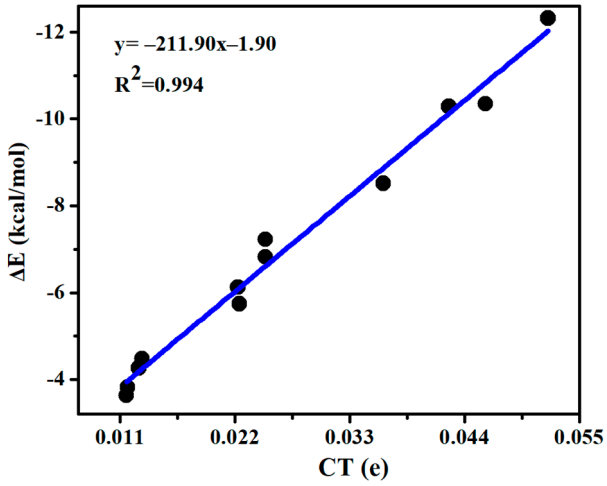

Figure 4. Interaction energy (ΔE) versus charge transfer (CT) in the chalcogen-bonded dyads.

The interaction energy was decomposed into electrostatic (E^{es}), exchange (E^{ex}), repulsion (E^{rep}), polarization (E^{pol}) and dispersion energies (E^{disp}), collected in Table 4. The total interaction energy obtained with GAMESS program is almost equal to that with Gaussian program. Among the three attractive terms (E^{es}, E^{pol}, and E^{disp}), E^{es} is largest, confirming that electrostatic interaction is dominant. This conclusion is further confirmed by the linear relationship between the total interaction energy and the electrostatic interaction (Figure S4). No linear relationship is present between the total interaction energy and the other attractive terms. Politzer and co-authors explained most σ-hole interactions by means of Coulombic interactions and concluded that charge transfer is an extreme form of polarization [45,46]. However, the interaction energy of chalcogen bond displays a good linear relationship with the charge transfer but not with polarization energy. Both E^{pol} and E^{disp} are comparable since the latter corresponds to 50–90% of the former.

Table 4. Electrostatic (E^{es}), exchange (E^{ex}), repulsion (E^{rep}), polarization (E^{pol}), and dispersion (E^{disp}) energies in the chalcogen-bonded dyads, all in kcal/mol.

	E^{es}	E^{ex}	E^{rep}	E^{pol}	E^{disp}	E_{total}
ChB-1	−35.30	−33.47	73.69	−10.38	−5.22	−10.68
ChB-2	−42.36	−39.88	90.26	−12.01	−8.70	−12.69
ChB-3	−28.83	−31.55	66.06	−9.64	−5.21	−9.17
ChB-4	−35.15	−38.04	80.26	−10.69	−7.00	−10.62
ChB-5	−22.40	−18.74	49.95	−9.00	−6.70	−6.89
ChB-6	−26.82	−23.50	62.09	−12.33	−6.92	−7.48
ChB-7	−20.27	−18.25	47.74	−8.48	−6.92	−6.18
ChB-8	−24.35	−22.38	57.20	−11.29	−6.95	−7.77
ChB-9	−13.07	−19.65	41.35	−7.31	−5.41	−4.09
ChB-10	−15.45	−18.49	43.39	−7.45	−6.63	−4.63
ChB-11	−12.28	−18.52	39.22	−6.90	−5.48	−3.96
ChB-12	−14.32	−17.57	41.47	−7.33	−6.58	−4.33

3.2. Cooperativity between Spodium and Chalcogen Bonds in Triads

Only three chalcogen-bonded dyads of ChB-1, ChB-2, and ChB-4 have a larger interaction energy exceeding 10 kcal/mol, thus we are interested in how to strengthen the ChB by adding a spodium bond (SpB) and its enhancing mechanism. Figure 5 shows the diagram of the ternary complex, where a M···N SpB coexists with a ChB and a HB. The formation of SpB can be understood by the MEP maps of MCO_3 and three N-bases (Figure S5), where a red region with positive MEPs and a blue one with negative MEPs are found on the M and N atoms, respectively. Since such M···N SpB was analyzed in the previous study [14], thus it is not studied here and our aim is to strengthen the chalcogen bond by means of

SpB. These triads are marked from T-1 to T-36. The molecular configuration in the triad is similar to that in the dyad. The angles of X-Se···O (α_1) and Se-H···O (α_2) are almost not changed in the triad relative to the dyad in spite of no regular variation (Table S1).

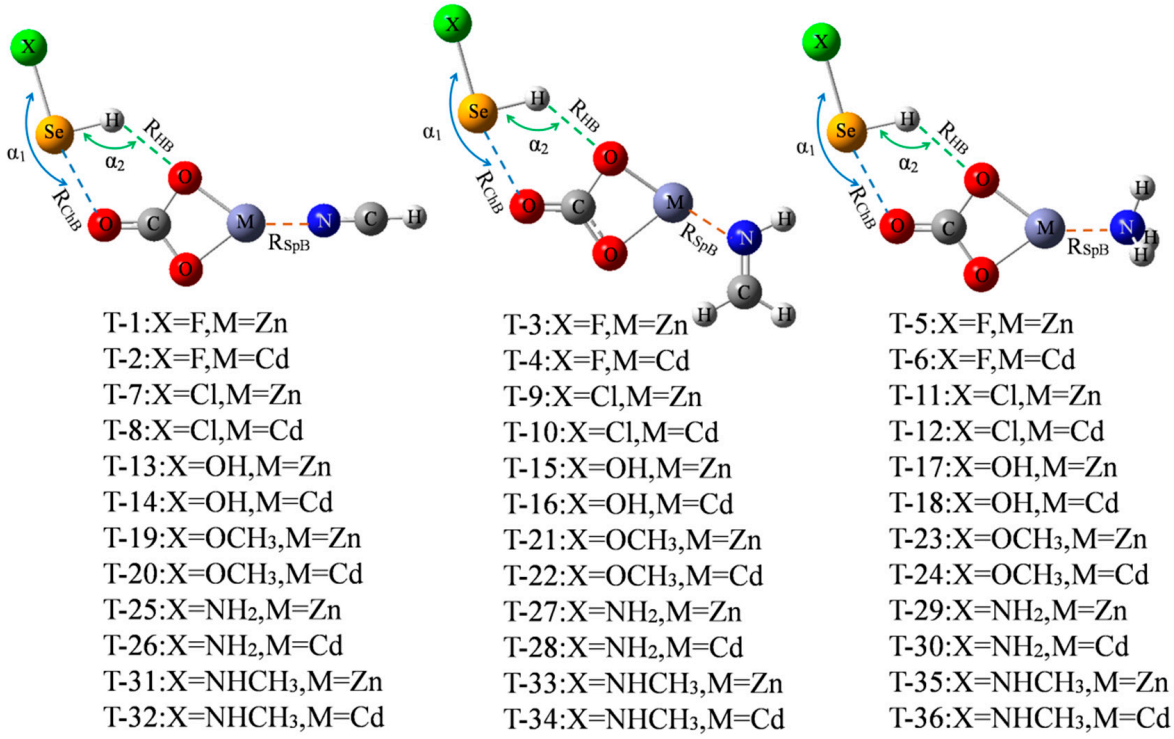

Figure 5. Schemes of XHSe-MCO_3-N-base ternary complexes.

Both the ChB and HB interactions are enhanced in the ternary complexes, which can be clearly evidenced by the shorter binding distances (Table 5). The shortening of both Se···O and H···O distances is very prominent and the largest shortening is up to 0.1 Å for each distance. The largest shortening of Se···O distance is found in the triads involving SeHCl. Therefore, an introduction of a spodium bond to MCO_3 leads to a prominent change in the binding distances of the ChB and HB though a slight change takes place for the angles of X-Se···O (α_1) and Se-H···O (α_2). The shortening of Se···O distance is larger than that of H···O distance in most triads excluding T-16 and from T-25 to T-36, and their largest difference is up to 0.057 Å. On the other hand, the SpB binding distance is also shortened in the triads although its shortening is much smaller than that of ChB and HB. This indicates that all bonds of ChB, HB, and SpB strengthened each other.

Table 5. Change of binding distance (ΔR, Å) in the triads relative to the corresponding dyads.

	ΔR_{ChB}	ΔR_{HB}	ΔR_{SpB}
HCN-$ZnCO_3$-SeHF(T-1)	−0.085	−0.070	−0.005
HCN-$CdCO_3$-SeHF(T-2)	−0.072	−0.051	−0.028
H_2CHN-$ZnCO_3$-SeHF(T-3)	−0.090	−0.072	−0.005
H_2CHN-$CdCO_3$-SeHF(T-4)	−0.082	−0.062	−0.018
H_3N-$ZnCO_3$-SeHF(T-5)	−0.093	−0.077	−0.006
H_3N-$CdCO_3$-SeHF(T-6)	−0.080	−0.061	−0.030
HCN-$ZnCO_3$-SeHCl(T-7)	−0.112	−0.071	−0.005
HCN-$CdCO_3$-SeHCl(T-8)	−0.100	−0.054	−0.027
H_2CHN-$ZnCO_3$-SeHCl(T-9)	−0.118	−0.071	−0.005
H_2CHN-$CdCO_3$-SeHCl(T-10)	−0.115	−0.058	−0.017

Table 5. *Cont.*

	ΔR_{ChB}	ΔR_{HB}	ΔR_{SpB}
H_3N-$ZnCO_3$-SeHCl(T-11)	−0.122	−0.080	−0.006
H_3N-$CdCO_3$-SeHCl(T-12)	−0.112	−0.056	−0.026
HCN-$ZnCO_3$-SeHOH(T-13)	−0.084	−0.083	−0.003
HCN-$CdCO_3$-SeHOH(T-14)	−0.072	−0.062	−0.025
H_2CHN-$ZnCO_3$-SeHOH(T-15)	−0.088	−0.085	−0.003
H_2CHN-$CdCO_3$-SeHOH(T-16)	−0.067	−0.070	−0.024
H_3N-$ZnCO_3$-SeHOH(T-17)	−0.092	−0.090	−0.004
H_3N-$CdCO_3$-SeHOH(T-18)	−0.080	−0.071	−0.027
HCN-$ZnCO_3$-$SeHOCH_3$(T-19)	−0.086	−0.082	−0.003
HCN-$CdCO_3$-$SeHOCH_3$(T-20)	−0.077	−0.053	−0.025
H_2CHN-$ZnCO_3$-$SeHOCH_3$(T-21)	−0.090	−0.084	−0.003
H_2CHN-$CdCO_3$-$SeHOCH_3$(T-22)	−0.071	−0.060	−0.024
H_3N-$ZnCO_3$-$SeHOCH_3$(T-23)	−0.095	−0.088	−0.003
H_3N-$CdCO_3$-$SeHOCH_3$(T-24)	−0.087	−0.065	−0.024
HCN-$ZnCO_3$-$SeHNH_3$(T-25)	−0.063	−0.085	−0.002
HCN-$CdCO_3$-$SeHNH_3$(T-26)	−0.046	−0.079	−0.023
H_2CHN-$ZnCO_3$-$SeHNH_3$(T-27)	−0.069	−0.085	−0.002
H_2CHN-$CdCO_3$-$SeHNH_3$(T-28)	−0.047	−0.075	−0.022
H_3N-$ZnCO_3$-$SeHNH_3$(T-29)	−0.066	−0.100	−0.002
H_3N-$CdCO_3$-$SeHNH_3$(T-30)	−0.049	−0.092	−0.024
HCN-$ZnCO_3$-$SeHNHCH_3$(T-31)	−0.061	−0.090	−0.002
HCN-$CdCO_3$-$SeHNHCH_3$(T-32)	−0.052	−0.073	−0.023
H_2CHN-$ZnCO_3$-$SeHNHCH_3$(T-33)	−0.067	−0.088	−0.002
H_2CHN-$CdCO_3$-$SeHNHCH_3$(T-34)	−0.049	−0.066	−0.022
H_3N-$ZnCO_3$-$SeHNHCH_3$(T-35)	−0.063	−0.106	−0.002
H_3N-$CdCO_3$-$SeHNHCH_3$(T-36)	−0.035	−0.092	−0.027

The first column in Table 6 is the total interaction energy of triad, ranging from −37.36 kcal/mol in T-36 to −68.28 kcal/mol in T-3. The interaction energy between SeHX and the N base (ΔE_{far}) was deducted in calculating the interaction energies of SpB and ChB although this value is very small (<0.4 kcal/mol). Both ΔE_{SpB} and ΔE_{ChB} are increased in the triads relative to the corresponding dyads and their increase is almost equal in most triads. However, the increased percentage is larger for ΔE_{ChB} due to its smaller crude value. This shows that the enhancement of ChB and HB is larger than that of SpB, which supports the previous conclusion that the stronger interaction has a larger effect on the weaker one [47]. Similarly, the largest increased percentage of ChB interaction energy is found in the triads involving SeHCl.

Table 6. Total interaction energy (ΔE_{total}), interaction energy between molecular pairs (ΔE), and cooperative energy (E_{coop}) in the ternary complexes, all in kcal/mol.

	ΔE_{total}	ΔE_{SpB}	ΔE_{ChB}	ΔE_{far}	$\Delta\Delta E_{SpB}$	$\Delta\Delta E_{ChB}$	E_{coop}
T-1	−53.24	−42.42	−14.43	−0.42	−3.97	−4.08	−4.02
T-2	−48.20	−35.42	−16.20	−0.36	−3.58	−3.88	−3.68
T-3	−68.28	−57.39	−14.57	−0.37	−3.94	−4.22	−4.11
T-4	−60.32	−47.48	−16.69	−0.34	−2.47	−4.37	−2.65
T-5	−67.86	−56.97	−14.96	−0.37	−6.57	−4.61	−6.74
T-6	−60.51	−47.66	−16.80	−0.31	−4.16	−4.48	−4.38
T-7	−51.05	−42.19	−12.26	−0.39	−3.74	−3.74	−3.69
T-8	−45.96	−35.30	−13.97	−0.33	−3.46	−3.69	−3.51
T-9	−66.07	−57.14	−12.37	−0.35	−3.69	−3.85	−3.75
T-10	−58.08	−47.35	−14.47	−0.31	−2.34	−4.18	−2.48
T-11	−63.42	−54.50	−12.61	−0.35	−4.10	−4.09	−4.15

Table 6. *Cont.*

	ΔE_{total}	ΔE_{SpB}	ΔE_{ChB}	ΔE_{far}	$\Delta\Delta E_{SpB}$	$\Delta\Delta E_{ChB}$	E_{coop}
T-12	−56.40	−45.65	−14.43	−0.29	−2.15	−4.14	−2.33
T-13	−47.07	−40.84	−8.40	−0.23	−2.39	−2.27	−2.26
T-14	−41.32	−34.00	−9.40	−0.19	−2.16	−2.17	−2.06
T-15	−62.12	−55.84	−8.47	−0.22	−2.39	−2.34	−2.32
T-16	−54.32	−47.02	−9.23	−0.17	−2.01	−2.00	−1.91
T-17	−59.29	−53.03	−8.63	−0.21	−2.63	−2.50	−2.55
T-18	−53.44	−46.08	−9.79	−0.17	−2.58	−2.56	−2.54
T-19	−46.64	−40.78	−7.98	−0.21	−2.33	−2.24	−2.24
T-20	−40.89	−33.97	−8.97	−0.18	−2.13	−2.15	−2.05
T-21	−61.71	−55.80	−8.05	−0.21	−2.35	−2.31	−2.31
T-22	−53.91	−47.01	−8.80	−0.17	−2.00	−1.98	−1.91
T-23	−58.84	−52.96	−8.18	−0.19	−2.56	−2.44	−2.51
T-24	−53.01	−46.06	−9.35	−0.15	−2.56	−2.53	−2.54
T-25	−43.72	−39.89	−5.14	−0.09	−1.44	−1.32	−1.36
T-26	−37.61	−33.13	−5.74	−0.07	−1.29	−1.26	−1.22
T-27	−58.74	−54.86	−5.14	−0.09	−1.41	−1.32	−1.38
T-28	−50.72	−46.21	−5.59	−0.06	−1.20	−1.11	−1.17
T-29	−55.96	−54.14	−5.37	−0.11	−3.74	−1.55	−1.63
T-30	−49.54	−45.06	−6.00	−0.09	−1.56	−1.52	−1.47
T-31	−43.48	−39.86	−4.90	−0.08	−1.41	−1.28	−1.33
T-32	−37.36	−33.11	−5.50	−0.05	−1.27	−1.24	−1.21
T-33	−58.51	−54.84	−4.91	−0.08	−1.39	−1.29	−1.36
T-34	−50.50	−46.21	−5.36	−0.06	−1.20	−1.10	−1.17
T-35	−55.60	−51.99	−5.05	−0.10	−1.59	−1.43	−1.48
T-36	−49.17	−43.62	−5.37	−0.06	−0.12	−1.11	−1.35

The interplay between different types of bonds in the triad can be estimated with cooperative energy (E_{coop}), which was calculated with the formulas of $E_{coop} = \Delta E_{total,T} - \Delta E_{ChB,D} - \Delta E_{SpB,D} - \Delta E_{far}$, in which $\Delta E_{total,T}$ is the total interaction energy of a triad, $\Delta E_{ChB,D}$ the interaction energy of the optimized chalcogen-bonded dyad, and $\Delta E_{SpB,D}$ the interaction energy of the optimized spodium-bonded dyad. This value is positive in all triads, confirming the positive cooperativity. Moreover, E_{coop} accounts for 2–10% of the total interaction energy, and this ratio falls within 6% of HB cooperativity [48].

The enhancement of ChB and SpB can also be confirmed by the larger electron densities at the Se···O and M···N BCPs of chalcogen and spodium bonds in the ternary systems compared to their binary analogues (Table S2). Interestingly, the largest increase in the electron density at the Se···O BCP is found in the triads involving SeHCl. Both Laplacians and energy densities are also varied in the triads, but no essential change is found in most triads with an exception in the triads involving SeHCl (Table S3). For the latter, the energy density at the Se···O BCP varies from positive in the chalcogen-bonded dyad to negative in the triad.

As presented in Table S4, both the positive MEP on the M atom and the negative MEP on the O atom of MCO_3 are increased when it forms a chalcogen bond and a spodium bond, respectively. This means that the M atom of MCO_3 in the chalcogen-bonded dyad engages in a stronger SpB, while the O atom of MCO_3 in the spodium-bonded dyad participates in a stronger ChB and HB. Thus, the positive cooperativity can be explained by a "pull-push" model, in which the SeHX molecule draws more electrons and the N-containing base donates more electrons simultaneously in the ternary complexes. The increase of ΔE_{ChB} in the triad is attributed to the contribution from the ChB and HB interactions, thus we explore the relationship between the increase of electron density at the Se···O BCP ($\Delta\rho_{ChB}$, Table S2) and the increase of negative MEP on the O atom of spodium-bonded dyad ($\Delta V_{S,min}$, Table S4). However, no consistent change is found between both terms, and even a reverse change is observed for them. For example, with the increase of $\Delta V_{S,min}$ on the O atom from H_3N-$ZnCO_3$ to H_2CHN-$ZnCO_3$ to HCN-$ZnCO_3$, $\Delta\rho_{ChB}$ is reduced

from 0.0079 a.u. in T = 6 to 0.0075 a.u. in T = 3 to 0.0071 a.u. in T-1. Thus the electrostatic interaction is only used to explain qualitatively the enhancement of ChB by the SpB.

Table S4 presents the charge transfer between MCO_3 and SeHX (CT_{ChB}) as well as between MCO_3 and N-base (CT_{SpB}) in the triads. CT_{SpB} exceeds 0.1e in most triads and is much bigger than CT_{ChB}. CT_{ChB} is half of CT_{SpB} for the strong ChB, while the former is less than 10% of the latter for the weak ChB. Both CT_{ChB} and CT_{SpB} are increased in the triads relative to the dyads. Moreover, the increase of CT_{ChB} is much larger than that of CT_{SpB}. Being consistent with the increase of the chalcogen bonding interaction energy, the increase of charge transfer for the ChB is largest in the triads involving SeHCl. A linear relationship is found between the increase of CT_{ChB} and the increase of chalcogen-bonded interaction energy (Figure 6), thus the enhancement of ChB and HB is attributed to the increase of charge transfer.

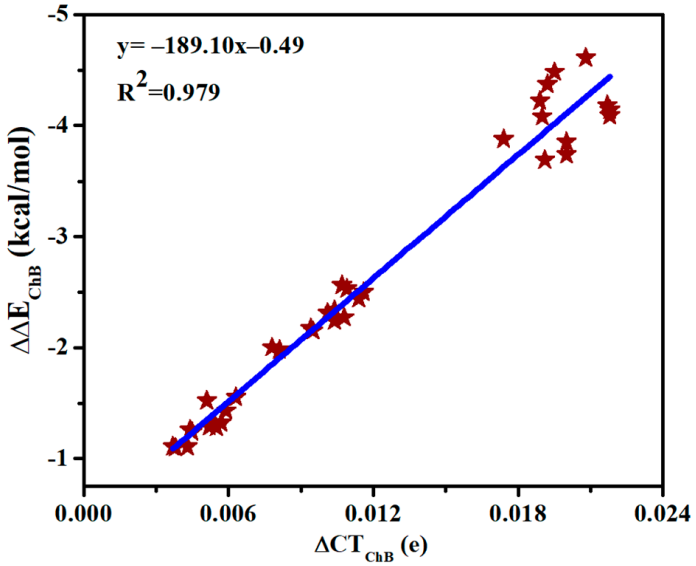

Figure 6. Relationship between increase of both charge transfer (ΔCT) and interaction energy (ΔΔE) in the chalcogen bonds.

4. Conclusions

Systematic theoretical calculations were performed to study the ternary complex of N-base-MCO_3-SeHX (X = F, Cl, OH, OCH_3, NH_2, $NHCH_3$; M = Zn, Cd; N-base = HCN, $NHCH_2$, and NH_3) and their corresponding binary analogues. Carbonate MCO_3 can form not only a spodium bond with the N-base but also a chalcogen bond with SeHX. The spodium bond is stronger than the chalcogen bond since the Zn(II) and Cd(II) are metal cations in the neutral carbonate salts. The chalcogen-bonded dyad is more stable in the sequence of F > Cl > OH > OCH_3 > NH_2 > $NHCH_3$ and $CdCO_3$ > $ZnCO_3$. The interaction energy of chalcogen-bonded dyad is greatly affected by the substituent X of SeHX, becoming more negative from −3.6 kcal/mol in $ZnCO_3$-$SeHNHCH_3$ to −12.3 kcal/mol in $CdCO_3$-SeHF. Both electrostatic and charge transfer interactions are responsible for the stability of chalcogen-bonded dyad. Both chalcogen and spodium bonds strengthened each other in N-base-MCO_3-SeHX, and the enhancing effect is larger for the chalcogen bond, which is mainly attributed to the increase of charge transfer.

Supplementary Materials: The following are available online. Table S1 Angles (α, deg) and binding distances (R, Å) in the ternary complexes as well as their difference (Δ) relative to the binary analogues. Table S2 Electron densities (ρ, au) at the intermolecular BCPs in the ternary systems and their change (Δρ, au) relative to the binary analogues. Table S3 Laplacians (∇2ρ) and energy densities (H) at the intermolecular Se···O and M···N BCPs in the ternary complexes, all in au. Table S4 The most negative MEP ($V_{S,min}$) on the O atom of C=O bond in the spodium-bonded binary complex and the most positive MEP ($V_{S,max}$) on the M atom in the chalcogen-bonded binary complex as well as their difference (ΔV) relative to the corresponding monomers, all in kcal/mol. Table S5 Charge transfer (CT, e) of chalcogen and spodium bonds in the ternary complexes and its change (ΔCT, e) relative to the binary analogues. Figure S1 Relationship between both angles of Se-H···O (α2) and X-Se···O (α1). Figure S2 Non-covalent interaction (NCI) maps of the chalcogen-bonded dyads. Blue, green, and red areas correspond to strong attractive, weak attractive and strong repulsion interactions, respectively. Figure S3 Interaction energy (ΔE) versus second-order perturbation energy (E(2)) of LpO→σ*Se-X orbital interaction in the chalcogen-bonded dyads. Figure S4 Interaction energy (ΔE) versus a) electrostatic energy (Ees), b) polarization energy (Epol), and c) dispersion energy (Edisp) in the chalcogen-bonded dyads. Figure S5 MEP maps on the 0.001 electrons Bohr−3 isodensity surface of monomers. Red and blue regions represent positive and negative MEPs, respectively. All are in kcal/mol.

Author Contributions: Q.L. conceived of the idea for this project and wrote a first draft of the manuscript; N.L. carried out the calculations and compiled the data; X.X. supervised the calculations and helped with a final draft. All authors have read and agreed to the published version of the manuscript.

Funding: This research was funded by the National Natural Science Foundation of China grant number (21573188 and 22103067).

Institutional Review Board Statement: Not applicable.

Informed Consent Statement: Not applicable.

Data Availability Statement: Not applicable.

Conflicts of Interest: The author declares no conflict of interest.

Sample Availability: Not applicable.

References

1. Lin, Y.F.; Aarts, M.G.M. The molecular mechanism of zinc and cadmium stress response in plants. *Cell. Mol. Life Sci.* **2012**, *69*, 3187–3206. [CrossRef] [PubMed]
2. Shen, Y.; Zhao, S.; Luo, J. The role of cations in second-order nonlinear optical materials based on π-conjugated $[BO_3]^{3-}$ groups. *Coord. Chem. Rev.* **2018**, *366*, 1–28. [CrossRef]
3. Yang, Y.; Dong, X.; Pan, S.; Wu, H. The rubidium barium borate resulting from B_7O_{15} fundamental building block exhibits DUV cutoff edge. *Inorg. Chem.* **2018**, *57*, 13380–13385. [CrossRef] [PubMed]
4. Xia, M.J.; Li, R.K. Crystal structure, growth and characterization of $LiPbB_9O_{15}$: A new congruent melting nonlinear optical crystal. *J. Solid State Chem.* **2013**, *201*, 288–292. [CrossRef]
5. Than, T.T.; Young, J.; Rondinelli, J.M.; Halasyamani, P.S. Mixed-metal carbonate fluorides as deep-ultraviolet nonlinear optical materials. *J. Am. Chem. Soc.* **2017**, *139*, 1285–1295.
6. Zou, G.; Ok, K.M. Novel ultraviolet (UV) nonlinear optical (NLO) materials discovered by chemical substitution-oriented design. *Chem. Sci.* **2020**, *11*, 5404–5409. [CrossRef] [PubMed]
7. Gong, P.; Liu, X.; Kang, L.; Lin, Z. Inorganic planar π-conjugated groups in nonlinear optical crystals: Review and outlook. *Inorg. Chem. Front.* **2020**, *7*, 839–952. [CrossRef]
8. Sharma, Y.; Sharma, N.; Rao, G.; Chowdari, B. Nano-$(Cd_{1/3}Co_{1/3}Zn_{1/3})$ CO_3: A new and high capacity anode material for Li-ion batteries. *J. Mater. Chem.* **2009**, *19*, 5047–5054. [CrossRef]
9. De Beauvoir, T.H.; Sangregorio, A.; Cornu, I.; Josse, M. Synthesis, sintering by Cool-SPS and characterization of $A_2Cu(CO_3)_2$ (A= K, Na): Evidence for multiferroic and magnetoelectric cupricarbonates. *Dalton Trans.* **2020**, *49*, 7820–7828. [CrossRef] [PubMed]
10. Karuppaiah, M.; Akilan, R.; Sakthivel, P.; Asaithambi, S.; Shankar, R.; Yuvakkumar, R.; Ravi, G. Synthesis of self-assembled micro/nano structured manganese carbonate for high performance, long lifespan asymmetric supercapacitors and investigation of atomic-level intercalation properties of OH^- ions via first principle calculation. *J. Energy Storage* **2020**, *27*, 101138. [CrossRef]
11. Alkorta, I.; Elguero, J.; Frontera, A. Not only hydrogen bonds: Other noncovalent interactions. *Crystals* **2020**, *10*, 180. [CrossRef]

12. Bauzá, A.; Alkorta, I.; Elguero, J.; Mooibroek, T.J.; Frontera, A. Spodium bonds: Noncovalent interactions involving group 12 elements. *Angew. Chem Int. Ed.* **2020**, *59*, 17482–17487. [CrossRef] [PubMed]
13. Xia, T.; Li, D.; Cheng, L. Theoretical analysis of the spodium bonds in $HgCl_2 \cdots L$ (L= ClR, SR_2, and PR_3) dimers. *Chem. Phys.* **2020**, *539*, 110978. [CrossRef]
14. Liu, N.; Li, Q.Z. Group 12 carbonates and their binary complexes with nitrogen bases and FH_2Z molecules (Z= P, As, and Sb); synergism in forming ternary complexes. *ChemPhysChem* **2021**, *22*, 1698–1705. [CrossRef]
15. Wang, W.; Ji, B.; Zhang, Y. Chalcogen bond: A sister noncovalent bond to halogen bond. *J. Phys. Chem. A* **2009**, *113*, 8132–8135. [CrossRef] [PubMed]
16. Clark, T.; Hennemann, M.; Murray, J.S.; Politzer, P. Halogen bonding: The σ-hole. *J. Mol. Model.* **2007**, *13*, 291–296. [CrossRef]
17. Murray, J.S.; Lane, P.; Clark, T.; Politzer, P. σ-Hole bonding: Molecules containing group VI atoms. *J. Mol. Model.* **2007**, *13*, 1033–1038. [CrossRef] [PubMed]
18. Politzer, P.; Murray, J.S.; Clark, T. Halogen bonding and other σ-hole interactions: A perspective. *Phys. Chem. Chem. Phys.* **2013**, *15*, 11178–11189. [CrossRef] [PubMed]
19. Politzer, P.; Murray, J.S.; Clark, T.; Resnati, G. The σ-hole revisited. *Phys. Chem. Chem. Phys.* **2017**, *19*, 32166–32178. [CrossRef] [PubMed]
20. Iwaoka, M.; Komatsu, H.; Katsuda, T.; Tomoda, S. Nature of nonbonded $Se \cdots O$ interactions characterized by ^{17}O NMR spectroscopy and NBO and AIM analyses. *J. Am. Chem. Soc.* **2004**, *126*, 5309–5317. [CrossRef] [PubMed]
21. Haberhauer, G.; Gleiter, R. The nature of strong chalcogen bonds involving chalcogen-containing heterocycles. *Angew. Chem. Int. Ed.* **2020**, *59*, 21236–21243. [CrossRef] [PubMed]
22. Mahadevi, A.S.; Sastry, G.N. Cooperativity in noncovalent interactions. *Chem. Rev.* **2016**, *116*, 2775–2825. [CrossRef] [PubMed]
23. Alkorta, I.; Blanco, F.; Deyà, P.M.; Elguero, J.; Estarellas, C.; Frontera, A.; Quinonero, D. Cooperativity in multiple unusual weak bonds. *Theor. Chem. Acc.* **2010**, *126*, 1–14. [CrossRef]
24. Zierkiewicz, W.; Wysokiński, R.; Michalczyk, M.; Scheiner, S. Chalcogen bonding of two ligands to hypervalent YF_4 (Y = S, Se, Te, Po). *Phys. Chem. Chem. Phys.* **2019**, *21*, 20829–20839. [CrossRef]
25. Esrafili, M.D.; Mohammadian-Sabet, F. Ab initio calculations of cooperativity effects on chalcogen bonding: Linear clusters of $(OCS)_{2–8}$ and $(OCSe)_{2–8}$. *Struct. Chem.* **2015**, *26*, 199–206. [CrossRef]
26. Jeannin, O.; Huynh, H.T.; Riel, A.; Fourmigue, M. Chalcogen bonding interactions in organic selenocyanates: From cooperativity to chelation. *New J. Chem.* **2018**, *42*, 10502–10509. [CrossRef]
27. Guo, X.; An, X.L.; Li, Q.Z. $Se \cdots N$ chalcogen bond and $Se \cdots X$ halogen bond involving F_2C=Se: Influence of hybridization, substitution, and cooperativity. *J. Phys. Chem. A* **2015**, *119*, 3518–3527. [CrossRef] [PubMed]
28. Li, Q.Z.; Li, R.; Guo, P.; Li, H.; Li, W.Z.; Cheng, J.B. Competition of chalcogen bond, halogen bond, and hydrogen bond in SCS-HOX and SeCSe-HOX (X = Cl and Br) complexes. *Comput. Theor. Chem.* **2012**, *980*, 56–61. [CrossRef]
29. Mó, O.; Montero-Campillo, M.M.; Alkorta, I.; Elguero, J.; Yáez, M. Ternary complexes Stabilized by chalcogen and alkaline-earth bonds: Crucial role of cooperativity and secondary noncovalent interactions. *Chem. Eur. J.* **2019**, *25*, 11688–11695. [CrossRef] [PubMed]
30. Saberinasab, M.; Salehzadeh, S.; Solimannejad, M. The effect of a strong $cation \cdots \pi$ interaction on a weak $selenium \cdots \pi$ interaction: A theoretical study. *Comput. Theor. Chem.* **2016**, *1092*, 41–46. [CrossRef]
31. Frisch, M.J.; Trucks, G.W.; Schlegel, H.B.; Scuseria, G.E.; Robb, A.; Cheeseman, J.R.; Scalmani, G.; Barone, V.; Mennucci, B.; Petersson, G.A.; et al. *Gaussian 09, RevisionD.01*; Gaussian Inc.: Wallingford, CT, USA, 2009.
32. Schuchardt, K.L.; Didier, B.T.; Elsethagen, T.; Sun, L.; Gurumoorthi, V.; Chase, J.; Windus, T.L. Basis set exchange: A community database for computational sciences. *J. Chem. Inf. Model.* **2007**, *47*, 1045–1052. [CrossRef]
33. Boys, S.F.; Bernardi, F. The calculation of small molecular interactions by the differences of separate total energies. Some procedures with reduced errors. *Mol. Phys.* **1970**, *19*, 553–566. [CrossRef]
34. Bulat, F.A.; Toro-Labbé, A.; Brinck, T.; Murray, J.S.; Politzer, P. Quantitative analysis of molecular surfaces: Areas, volumes, electrostatic potentials and average local ionization energies. *J. Mol. Model.* **2010**, *16*, 1679–1691. [CrossRef] [PubMed]
35. Keith, T.A. *AIMALL, Version 13.05.06*; TK Gristmill Software: Overland Park, KS, USA, 2013.
36. Glendening, E.D.; Badenhoop, J.K.; Reed, A.E.; Carpenter, J.E.; Bohmann, J.A.; Morales, C.M.; Landis, C.R.; Weinhold, F. NBO 5.0. Available online: https://www.scm.com/wp-content/uploads/pdfs/2012/nbo5_man.pdf (accessed on 22 May 2021).
37. Glendening, E.D.; Badenhoop, J.K.; Reed, A.E.; Carpenter, J.E.; Bohmann, J.A.; Morales, C.M.; Landis, C.R.; Weinhold, F. NBO 6.0. Available online: https://www.scm.com/doc/ADF/_downloads/8444f25334aca639d7f8a39b9d0a1a04/nbo6_manual.pdf (accessed on 22 May 2021).
38. Lu, T.; Chen, F. Multiwfn: A multifunctional wavefunction analyzer. *J. Comput. Chem.* **2012**, *33*, 580–592. [CrossRef] [PubMed]
39. Humphrey, W.; Dalke, A.; Schulten, K. VMD: Visual molecular dynamics. *J. Mol. Graph.* **1996**, *14*, 33–38. [CrossRef]
40. Contreras-Garcia, J.; Johnson, E.R.; Keinan, S.; Robin, C.; Jean-Philip, P.; Beratan, D.N.; Yang, W.T. NCIPLOT: A program for plotting noncovalent interaction regions. *J. Chem. Theory Comput.* **2011**, *7*, 625–632. [CrossRef]
41. Su, P.F.; Li, H. Energy decomposition analysis of covalent bonds and intermolecular interactions. *J. Chem. Phys.* **2009**, *131*, 014102. [CrossRef]
42. Schmidt, M.W.; Baldridge, K.K.; Boatz, J.A.; Elbert, S.T.; Gordon, M.S.; Jensen, J.H.; Koseki, S.; Matsunaga, N.; Nguyen, K.A.; Su, S.; et al. General atomic and molecular electronic structure system. *J. Comput. Chem.* **1993**, *14*, 1347–1363. [CrossRef]

43. Li, Q.Z.; An, X.L.; Luan, F.; Li, W.Z.; Gong, B.A.; Cheng, J.B. Regulating function of methyl group in strength of CH···O hydrogen bond: A high-level ab initio study. *J. Phys. Chem. A* **2008**, *112*, 3985–3990. [CrossRef]
44. Shukla, R.; Chopra, D. Exploring the role of substitution on the formation of Se···O/N noncovalent bonds. *J. Phys. Chem. B* **2015**, *119*, 14857–14870. [CrossRef] [PubMed]
45. Clark, T.; Murray, J.S.; Politzer, P. A perspective on quantum mechanics and chemical concepts in describing noncovalent interactions. *Phys. Chem. Chem. Phys.* **2018**, *20*, 30076–30082. [CrossRef] [PubMed]
46. Politzer, P.; Murray, J.S.; Clark, T. Mathematical modeling and physical reality in noncovalent interactions. *J. Mol. Model.* **2015**, *21*, 52. [CrossRef]
47. Zhang, J.R.; Li, W.Z.; Cheng, J.B.; Liu, Z.B.; Li, Q.Z. Cooperative effects between π-hole triel and π-hole chalcogen bonds. *RSC Adv.* **2018**, *8*, 26580–26588. [CrossRef]
48. Rivelino, R.; Canuto, S. Theoretical study of mixed hydrogen-bonded complexes: $H_2O\cdots HCN\cdots H_2O$ and $H_2O\cdots HCN\cdots HCN\cdots H_2O$. *J. Phys. Chem. A* **2001**, *105*, 11260–11265. [CrossRef]